Indian Journal of Pure & Applied Physics
Vol. 62, November 2024, pp. 971-978
DOI: 10.56042/ijpap.v62i11.8697

A Simulation Study of Various ETL Layers to Design the High Performance Pb-Free perovskite ($FASnI_3$) Solar Cell

Khushboo Dixit & Gufran Ahmad*

Department of Electrical Engineering, Faculty of Engineering, Dayalbagh Educational Institute, Agra 282 005, India

Received 12 February 2024; accepted 10 October 2024

There are significant efforts being made to develop high-efficiency, lead-free perovskite solar cells (PSCs). In this study, Formamidinium tin iodide ($FASnI_3$) has been used as an absorber layer to design a stable lead-free PSC. $FASnI_3$ absorber has a wider band gap (1.41 eV) and is more temperature stable than lead-free Sn-based perovskite ($CH_3NH_3SnI_3$). In this work, 1-D device simulation has been performed using SCAPS to get the optimum performance of the lead-free $FASnI_3$-based PSCs. We have checked varieties of electron transport layers (ETL) such as WO_3, TiO_2, ZnO, PCBM, IGZO, ZnS, and WS_2 to find the maximum power conversion efficiency (PCE) from the $FASnI_3$ lead-free PSC. A detailed simulation study of the proposed solar cell architecture using SCAPS has been done to optimize the device structure and get the maximum power conversion efficiency. The proposed solar cell structure has shown an efficiency of 16% with a J_{SC} of 27.02 mA, V_{oc} of 0.925V, and FF of 63.98% which is the highest among the $FASnI_3$ based lead-free solar cell structures to date.

Keywords: Perovskite; Tungsten Oxide; Cadmium; Electron affinity; Band gap; Power conversion efficiency

1 Introduction

It has been proven that the large emissions of greenhouse gases due to the burning of fossil fuels are the main cause of global warming. The effects of global warming and climate change due to large emissions of CO_2 in the atmosphere are clearly visible and are now critical to protecting humans, wildlife, aquatic life, and ecosystems. Harvesting the energy from the sun is clearly a way to mitigate global warming while also promising to produce a low-cost, clean, and sustainable energy supply for the world. Crystalline silicon (C-Si)-based PV modules are dominating the market due to their reliability and mature fabrication process. However, the levelized cost of electricity (LCOE) for crystalline PV modules is still high. Therefore, to reduce the LCOE, we must increase the cell efficiency and use low-cost materials and processing. Thin film solar cells (TFSCs) technology is one of the best alternatives to C-Si PV in terms of cost and manufacturing processes. Among the TFSC, perovskite-based solar cells have been proven to be highly promising in terms of cost and PCE and have been widely investigated. However, the presence of toxic lead (Pb) elements in perovskite materials has limited its wide acceptance in large-scale perovskite solar cell industries due to environmental challenges. Therefore, the current focus of the research community is to design Pb-free PSCs with high efficiency and stability.

A perovskite is essentially any RMX_3 compound[1]. (R is the alkyl group, M is metal, and X is halogen). Its large electron diffusion length, high optical absorption, and low processing temperature make it suitable for solar cells[2]. Halide perovskite has recently demonstrated promising results in solar cell technology, therefore attracting a lot of attention now due to its hybrid nature, low processing costs, and higher power conversion efficiency. Despite lead-based perovskite's reported high-power conversion efficiency (PCE), which exceeds 20%[3], instability and toxicity are causes for concern with lead. To lessen the toxicity of metal halide perovskite, two methods are presented.

In the first method, lead is combined with less toxic metals, such as tin-lead alloyed perovskite ($CH_3NH_3Sn_xPb_{1-x}$)[4,5]. The second method involves completely swapping out lead for similar metals. Additionally, temperature instability is the main issue that plagues $CH_3NH_3SnI_3$ and $CsSnI_3$[6,7], despite the positive absorbing characteristics of those materials. The organic cation used in perovskite is the cause of this instability problem. Formamidinium HC $(NH_2)_2$ has been found to introduce a more solid perovskite structure, leading to the introduction of more stable

*Corresponding author: (E-mail: gufranahmad@dei.ac.in)

materials[8]. The formamidinium tin iodide absorber (HC $(NH_{2)2}SnI_3$-$FASnI_3$) has an energy band gap of 1.41 eV and absorbs wavelengths up to 880 nm. The most popular electron transport material in PSC up to this point has been TiO_2, which produced good results but also had some drawbacks like its early degradation over time under prolonged UV illumination and the oxygen vacancy that would activate the surface traps. Therefore, it is necessary to explore some new ETL materials to get more stable solar cells[9].

WO_3 thin films have already been used and reported in a number of other papers. Because of its characteristics, such as a tunable bandgap (2.6–3.5 eV)[10], which corresponds to a wavelength of 475 nm, it can absorb light in the visible spectrum. Additionally, it has a noticeable transmittance of 80% in the visible region, giving fierce competition to the traditional TiO_2 layer[11].

In addition, Formamidinium $HC(NH_2)_2$ is preferred over other perovskite absorber layerbecause it is more stable than conventional $CH_3NH_3SnI_3$[12]. Despite having promising absorbing qualities, $CH_3NH_3SnI_3$ has a major temperature instability problem. The organic cation used in perovskite is the cause of this instability problem. Formamidinium $HC(NH_2)_2$ has been found to introduce a more solid perovskite structure, leading to the introduction of more stable materials[13].

2 Simulation Technique and Device Design

The structure of the proposed solar cell is shown in Fig. 1. The device structure is n-i-p type, where the n-layer consists of the ETL, the p-region is the HTL, and the i-region is the intrinsic region. In our work, we have attempted to optimise the solar cell output parameters using various ETLs and compared the PV parameters. P-type Spiro-O-MeTAD was used as the HTL.

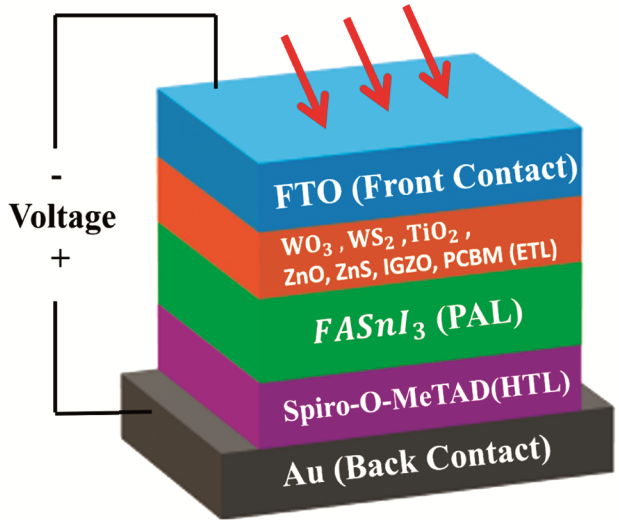

Fig. 1 — Schematic diagram of simulated structure

All the simulations were performed using SCAPS 1-D. The simulations were performed at standard illumination conditions of 1000 W/m^2 and 300 K in the AM 1.5 g spectrum. The following equation was used to calculate the absorption coefficient[14]:

$$\alpha(E) = \left(\alpha_o + \beta_o \frac{E_g}{h\nu}\right)\sqrt{\frac{h\nu}{E_g} - 1} \quad \ldots (1)$$

The following semiconductor equations used in SCAPS are the foundation for this simulation work: (i) Poisson's equation; (ii) the electron-hole continuity equation. The following is Poisson's equation:

$$\frac{d}{dx}\left(-\varepsilon(x)\frac{d\varphi}{dx}\right) = \left[p(x) - n(x) + N_D(x) - N_A(x) + p(x) - n(x)\right] \quad \ldots (2)$$

where n(x) and p(x) are the trapped electron and hole densities, p is the free hole density, N_D is the donor density, NA is the acceptor density, n(x) and p(x) are the free electron and hole densities, and is the medium's dielectric constant.

The 1-D continuity equation for electrons and holes is given as:

For electrons:

$$\frac{\partial n(x,t)}{\partial t} = \frac{1}{q}\frac{\partial Jn}{\partial x} + G_n(x,t) - R_n(x,t) \quad \ldots (3)$$

For holes:

$$\frac{\partial p(x,t)}{\partial t} = \frac{1}{q}\frac{\partial Jp}{\partial x} + G_p(x,t) - R_p(x,t) \quad \ldots (4)$$

Carrier density for electrons:

$$J_n = q\left(n\mu_n E + D_n \frac{dn}{dx}\right) \quad \ldots (5)$$

Carrier density for holes:

$$J_p = q\left(p\mu_p E + D_p \frac{dp}{dx}\right) \quad \ldots (6)$$

In steady state conditions $\frac{dn}{dt} = 0$. Hence

$$\frac{1}{q}\frac{\partial J_n}{\partial x} = -G_n(x,t) - R_n(x,t) \quad \ldots (7)$$

On substituting the value of j_n from the above equation we get

Table 1 — Material parameters of various layers used in the PSC simulation[15-18]

Parameters	FTO	$FASnI_3$	Spiro-O-MeTAD
W(μm)	0.500	0.600	0.020
E_g(eV)	3.5	1.52	3.5
χ (eV)	4.0	3.53	4.0
Ɛr	9.0	8.2	9.0
Nc (cm^{-3})	2.2×10^{18}	2.2×10^{17}	2.2×10^{17}
Nv (cm^{-3})	1.8×10^{19}	1.8×10^{19}	1.1×10^{19}
μ_e (cm^2/V-S)	20	2 x 10	2×10^2
μ_p (cm^2/V-S)	10	2 x 10	3×10^1
N_D (cm^{-3})	2×10^{19}	0	0
N_t (cm^{-3})	10^{15}	10^{15}	10^{15}
N_A (cm^{-3})	0	0	1×10^{18}

$$n\mu_n \frac{dE}{dx} + E\mu_n \frac{dn}{dx} + D_n \frac{d^2n}{dx^2} = -G_n(x,t) - R_n(x,t) \quad ...(8)$$

Similarly, for holes

$$-p\mu_p \frac{dE}{dx} - E\mu_p \frac{dp}{dx} + D_p \frac{d^2p}{dx^2} = -G_p(x,t) - R_p(x,t) \quad ... (9)$$

These coupled differential equations are solved by SCAPS, to find the unknown variables. Table-1 is showing all the parameters of layers used in simulation.

3 Results and Discussion

3.1 Absorber layer thickness variation impact on the performance of PCE

The thickness of the absorber layer Influences the response of the solar spectrum and plays a significant role in determining the efficiency of a perovskite solar cell. $FASnI_3$ has been used in thicknesses ranging from 500 nm to 1000 nm, with WO_3 serving as the ETL layer and spiro-OMeTAD as the layer. Here, the thickness of the absorber layer is varied by keeping other parameters constant. The outcome is displayed in Fig. 2. The short circuit current (Jsc) rises with increasing thickness because a thicker absorber layer will absorb more photons, which will lead to the formation of more electron-hole pairs. But as the charges must travel a greater distance for diffusion, the likelihood of recombination also rises with a thicker absorber layer. As a result, once a certain thickness is reached, efficiency starts to decline. The absorber layer's thickness needs to be chosen in such a way that the excess charge carrier's diffusion length is greater than the thickness. Due to the perovskite material's direct bandgap of 1.3 eV and high absorption coefficient of 10^5 cm^{-1}, high power conversion efficiency can be achieved with only a thin absorber layer (PCE). Reduced absorber layer

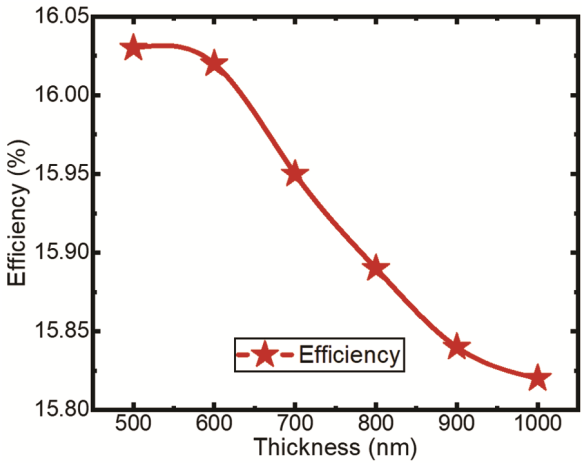

Fig. 2 — Effect of variation of thickness of absorber layer on the efficiency of PSC

thickness reduces absorption rate, which has a negative impact on efficiency, while increased thickness prevents charge carriers from ascending to the charge collecting layers. According to the simulation, a thickness of 600 nm to 700 nm would be adequate to absorb AM 1.5 G radiation. As shown in Fig. 2, a 650 nm-thick absorber layer is ideal to achieve high PCE for perovskite solar cells.

3.2 Impact of ETL and HTL thickness on the performance of PCE

In this study, the thickness of the Electron Transport Layer (ETL) and Hole Transport Layer (HTL) is varied from 10 nm to 100 nm, using the SCAPS-1D simulation tool. WO_3 is chosen as the ETL due to its favorable electron mobility. The primary function of an ETL is to efficiently block holes and transport electrons from the absorber layer to the cathode[22,23]. While varying the thickness of the ETL and HTL, the absorber layer thickness is maintained at its optimal value determined in the

previous section, with other parameters taken from Tables 1 & 3.

Initially, the thickness of WO_3 is varied while keeping the thickness of the HTL and absorber layer constant. From Table 2, we observe the effect of ETL thickness on the Power Conversion Efficiency (PCE) of the perovskite solar cell. If the thickness of the ETL is less than 20 nm, electrons may not be effectively collected and transported, leading to lower Jsc. Conversely, an excessively thick ETL may introduce resistance and hinder charge transport, resulting in lower PCE. This is primarily due to the uniform number of charge carriers produced in the lead-free perovskite material. The optimal thickness of the ETL in this simulation is 40 nm.

Next, the thickness of Spiro-O-MeTAD is varied from 10 to 100 nm while keeping all other parameters constant. Table 2 shows that as the thickness of the HTL is varied from 10 to 100 nm, Jsc also increases, virtually reaching a constant value. Increasing the thickness of the HTL can lead to higher optical absorption within the layer, resulting in a higher generation rate of electron-hole pairs and an increase in Jsc up to a certain point. It was found that increasing thickness also reduced the open-circuit voltage (Voc). Adjusting the HTL thickness can affect the energy level alignment at the interfaces and the charge transport properties within the device due to energy level mismatches and charge carrier recombination, leading to a decrease in Voc. In this study, the optimal thickness of the HTL is determined to be 70 nm.

Table 2 shows the different ETL parameters taken in this simulation. In this simulation, different ETLs are used by keeping other layers constant. $FASnI_3$ is used as an absorber layer, and Spiro-O-MeTAD is used as an HTL.

3.3 Effect of varying donor density of WO_3 layer on the PCE

Apart from the effect of thickness, the donor density of electrons in the ETL layer has a substantial impact on the photovoltaic cell's device performance. Donor density plays a crucial role in maximising a device's performance because an increase in doping means an increase in mobile carrier concentration. On the other hand, the motion impedance of the defects created by the doping atoms reduces mobility. Fermi level shifts towards the band edges with an increase in doping concentration, and as a result, the open circuit voltage of the solar cell increases. When doping

Table 2 — Impact of various ETL and HTL Thickness variation on the Device performance

Thickness of ETL/HTL layer (nm)	PCE (%) (HTL thickness is constant & ETL thickness is varied)	PCE (%) (ETL thickness is constant & HTL thickness is varied)
10	16.00	15.71
20	16.00	16.00
30	16.28	16.12
40	16.32	16.18
50	16.32	16.22
60	16.22	16.32
70	16.18	16.38
80	16.15	16.40
90	16.12	16.44
100	16.09	16.51

Table 3 — Simulation Parameters of different ETLs[24-31]

Parameters	WO_3	ZnO	TiO_2	PCBM	IGZO	ZnS	WS_2
W(nm)	20	20	20	20	20	20	20
E_g(eV)	2.6	3.3	3.20	2.10	3.55	3.7	2.3
χ (eV)	3.8	4.0	3.6	3.5	3.92	3.9	3.65
Ɛr	4.8	3.9	9.0	3.9	10	9.0	13.60
Nc (cm^{-3})	1×10^{21}	2.2×10^{18}	1.8×10^{20}	2.5×10^{21}	5×10^{16}	2.0×10^{17}	1.8×10^{20}
Nv (cm^{-3})	2×10^{20}	1.8×10^{19}	1.8×10^{18}	2.5×10^{21}	5×10^{17}	1.0×10^{18}	2.2×10^{18}
μ_e (cm^2/V-S)	50	100	0.006	0.002	15	100	100
μ_p (cm^2/V-S)	50	25	0.006	0.002	0.1	25	100
N_D (cm^{-3})	2×10^{19}	2.2×10^{19}	2.0×10^{19}	2.0×10^{19}	5×10^{20}	2.2×10^{19}	2.2×10^{19}
N_t (cm^{-3})	10^{15}	10^{15}	10^{15}	10^{15}	10^{15}	10^{15}	10^{15}

increases, the contact difference of potential in p-n homojunctions correspondingly increases. This ensures that the doping concentration in the solar cells' substrate and emitter layers is at its ideal level.

The simulation has been performed by varying the concentration of donor density in the WO_3 layer from $1x10^{15}$ to $1x10^{20}$ cm^3 to get the optimum donor concentration. Fig. 3 shows the effect of increasing the donor density of all ETLs on the performance of PSC. From this figure, it has been observed that the optimum doping concentration is 10^{16} cm^3. The efficiency of PSC is falling at higher doping concentrations as well as at lower doping concentrations.

3.4 Effect of temperature on the performance of solar cell

As a solar cell is installed in an open space that is exposed to the sun, higher temperatures are a cause for concern in some locations during the summer, where daytime temperatures peak at 325 K, which negatively impacts the performance of the PSC.

Figure 4 shows the effect of temperature on the Voc, Jsc, FF, and PCE of the solar cell. It is evident that as the temperature was raised, there was a significant decrease in the power conversion efficiency of PSC. At 250 K, PSC is showing a maximum efficiency of 18%, and at 350 K, it is showing an efficiency of 12.6%. When the temperature rises, Voc and FF decrease as a result of the thermal and photodissociation of the absorber layer and the ETL layer.

The absorption layer in PSCs is extremely sensitive to environmental factors like moisture, oxygen, and especially temperature[32]. $FASnI_3$ is the most temperature-stable absorber layer. Despite $FASnI_3$ other perovskite absorber layers with good absorbing abilities, like $CH_3NH_3SnI_3$ and $CsSnI_3$[33,34], are plagued by the main problem of temperature instability. As temperature increases, the Methylammonium-perovskite first breaks down into PbI_2, which linearly reduces the efficiency of related solar cells[35]. The organic cation used in perovskite is the cause of this instability problem. Formamidinium $HC(NH_2)_2$ has been found to introduce a more solid perovskite structure, leading to the introduction of more temperature-stable materials[36].

3.5 Impact of Transparent conductive oxides (TCO) on the performance of solar cell.

A transparent electrode is necessary for a photovoltaic device because it lets incoming light

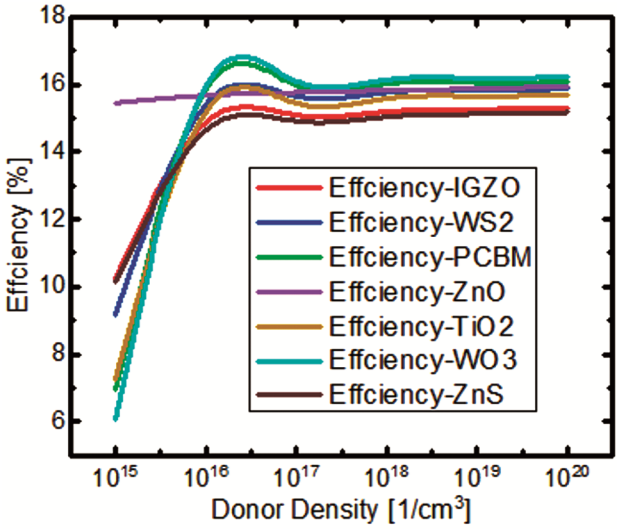

Fig. 3 — Donor density of all ETLs versus efficiency of PSC

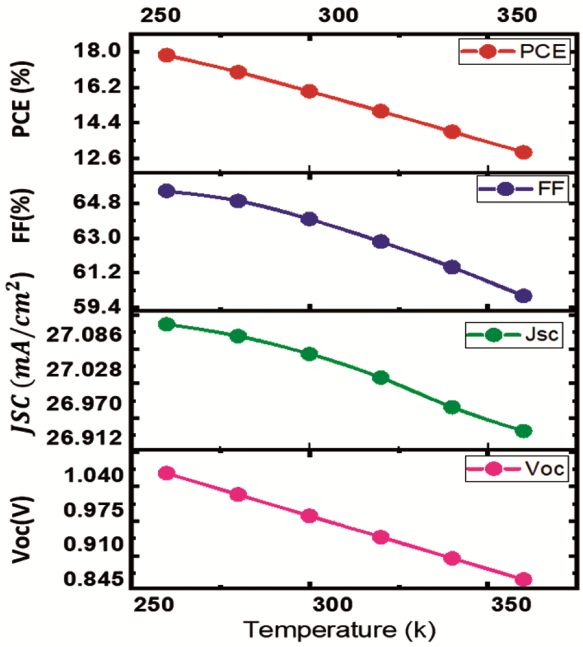

Fig. 4 — Effect of temperature variation on the performance of PSC

reach the photoactive layer. Due to their transparency and conductivity, transparent conductive oxides (TCO) like indium tin oxide (ITO), fluorine-doped tin oxide (FTO) and doped zinc oxide (ZnO) are excellent candidates for this use.

ZnO thin films have a high n-type conductivity electrically and are 85% optically transparent in the visible spectrum. Additionally, at room temperature, they have a large energy band gap of about 3.37 eV. Due to its wide band gap (3.37 eV), excellent optical and electrical properties, and abundance in the earth's

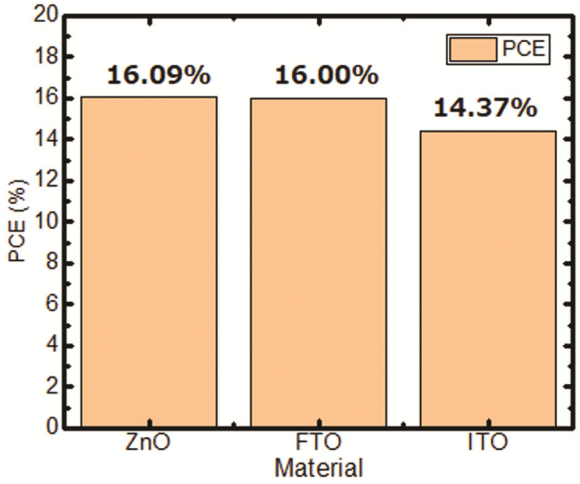

Fig. 5 — Efficiency shown by different TCO's

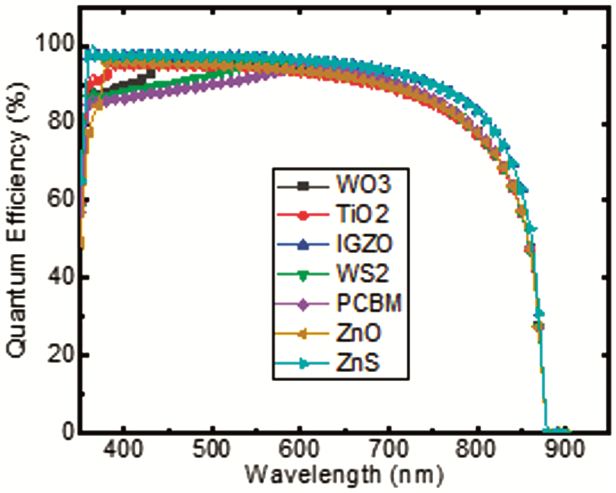

Fig. 6 — Quantum efficiency curve using various ETL

crust, ZnO can be used as TCO as an alternative to FTO and ITO[37]

In our designed structure, we have used ZnO, FTO, and ITO as TCOs and found that ZnO is performing best. Fig. 5 depicts that ZnO as a TCO is showing the highest power conversion efficiency of 16.09%, followed by FTO and ITO with efficiency of 16% and 14.37%, respectively.

3.6 Quantum efficiency of Perovskite solar cell

EQE represents the spectral response of various perovskite solar devices as a function of incident light wavelength. Fig. 6 displays the PSC QE curve for various ETL layers in the 300–900 nm wavelength range.

It is evident from Fig. 7 that QE values exceed 90%. From 350 to 400 nm, the QE increases with increasing wavelength. From 700 to 900 nm, the QE

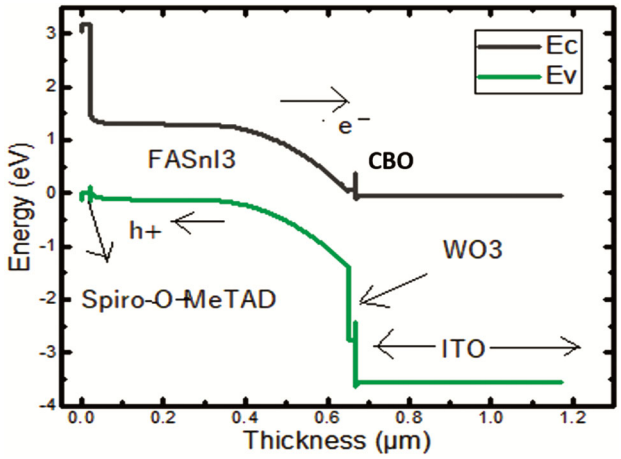

Fig. 7 — Band diagram of $FASnI_3$ devices with WO_3 as a ETLs

is nearly constant before gradually decreasing. The QE curve for WO_3 is almost identical to that of ZnO and TiO_2, paving the way for a new, inexpensive, and straightforward ETL layer replacement[38]. Additionally, it is possible to connect the EQE spectra to the observed short-circuit current densities using the equation in which F (λ) stands for photon flux and q for elementary charge[39].

$$J_{sc} = q\int f(\lambda).EQE(\lambda).d(\lambda) \quad \ldots (10)$$

Figure 7 displays the band alignment diagram for several ETL layers. ITO serves as the front contact in this diagram, underneath which are other ETL layers with clearly visible band alignment. A perovskite layer is formed by Formamidinium tin iodide ($FASnI_3$). According to simulation studies, WO_3 can be an excellent alternative to traditional TiO_2.

In the event that the conduction band offset (CBO) is too high in either direction, there will be band misalignments between the absorber and its junction partner. The unfavourable physical characteristics of interfacial layers often cause suboptimal band alignment, which reduces device performance due to increased charge carrier recombination. In Fig. 7, at the point where the absorber and ETL meet, there is a positive conduction band offset (CBO) of about 0.36 eV. This positive CBO causes a spike to form. This spike opposes the flow of photogenerated electrons towards the electrode[40].

Apart from their affinity, the conductivity of ETL and HTL is a crucial factor in cell design. It should be high from a conductivity standpoint in order to lower the cell's ohmic losses. It is possible to regulate the dopant types and thus the doping concentration of both HTL and ETL.

Table 4 — Impact of various ETL on the Device performance

Electro Transport Layers	Voc(V)	Jsc(mA/cm^2)	FF (%)	PCE (%)
WO_3	0.925	27.02	63.98	16.00
PCBM	0.924	26.75	64.27	15.89
IGZO	0.872	28.28	63.17	15.57
ZnO	0.888	27.02	64.45	15.51
ZnS	0.867	28.09	63.17	15.49
WS_2	0.880	26.94	65.11	15.45
TiO_2	0.925	26.91	64.61	15.21

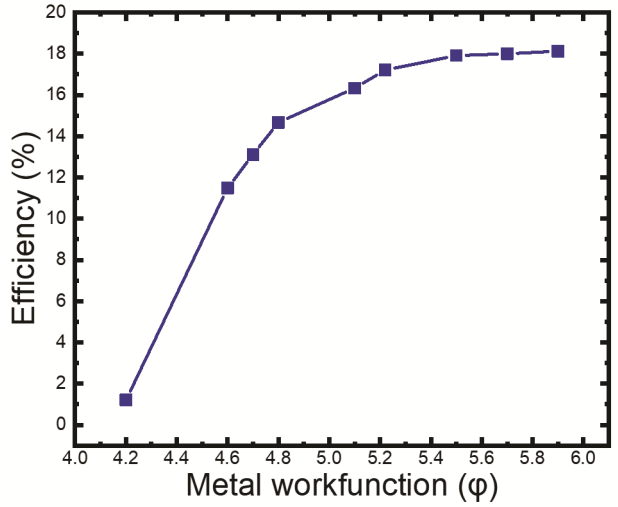

Fig. 8 — Impact of back metal work function on the power conversion efficiency of solar cell

Table 4 shows the result obtained by simulation of perovskite solar cells with different ETLs and TCOs. It is clear that the perovskite solar cell shows the highest efficiency when WO_3 is used as an electron transport layer. The second-highest efficiency is shown by the PCBM ETL architecture.

3.7 Effect of back contact work function

In this section, we present a comparative analysis of various metal back contacs employed in our study to evaluate their impact on perovskite solar cell (PSC) efficiency shown in Fig. 8. Metal contacts play a critical role in enhancing PSC performance, and our goal is to identify the most effective one for use with our $FASnI_3$-based perovskite solar cell. We tested silver, platinum, gold, nickel, and copper as back contacts to determine which metal yields the highest efficiency.

Our simulations reveal that platinum provides the highest power conversion efficiency (PCE) at 18.12 %, making it the most effective contact among those tested. In contrast, silver yielded the good efficiency, with a PCE of 16 %. Additionally, gold was also evaluated as a metal back contact in our simulation[41-44].

4 Conclusion

In this study, a simulation of a lead-free perovskite ($FASnI_3$) solar cell has been performed to show how different ETLs and TCOs as well as device parameters, affect cell performance. A detailed simulation is done to get a physical understanding of device performance. In this work, we investigated J-V characteristics, the band diagram, and quantum efficiency using various ETL layers. We also studied the impact of temperature, shallow donor density, thickness variation of the absorber, and ETL on the performance of PSC. The simulation of a perovskite solar cell using various ETL layers revealed that WO_3 was the most promising candidate and the best replacement for the traditional TiO_2 layer.

Furthermore, we draw the conclusion that a solar cell's performance is temperature sensitive. PCE is noticeable at lower temperatures, but it gradually deteriorates as the temperature rises. We analysed the effect of different TCOs on the performance of PSC. After simulation, we concluded that ZnO TCO could be a suitable alternative to ITO and FTO.

The parametric study shows that the final performance parameters of the intended solar cell are: a short-circuit current density (Jsc) of 27.02 mA/cm^2, an open-circuit voltage (Voc) of 0.92 V, a fill factor (FF) of 64%, and a power conversion efficiency (PCE) of 16%, which is the highest PCE of the FASnI3 absorber layer that has been reached so far. With respect to all other ETLs, the maximum PCE is achieved with the WO_3 layer. The optimum thickness of WO_3 (ETL) , absorber layer ($FASnI_3$), and Spiro-O-MeTAD (HTL) was found to be 40 nm, 70 nm and 600 nm–700 nm respectively.

References

1 Domanski K, Alharbi E A, Hagfeldt A, Grätzel M & Tress W, *Nat Energy*, 3, (2018) 61.

2 Jiang M, Niu Q, Tang X, Zhang H, Xu H, Huang W, Yao J, Yan B & Xia R, *Polymers (Basel)*, 11 (2019). 147.

3 Serrano-Lujan L, Espinosa N, Larsen-Olsen T T, Abad J, Urbina A & Krebs F C, *Adv Energy Mater*, 5 (2015) 1501119.

4 Ogomi Y, MORITA A, Tsukamoto S, Saitho T, Fujikawa N, Shen Q, *et al.*, *J Phys Chem Lett*, 5 (2014) 1004.
5 Hao C. Stoumpos C, Chang R P H & Kanatzidis M G, *J Am Chem Soc*, 136 (2014) 8094.
6 Kontos A G, Kaltzoglou A, Siranidi E, Palles D, Angeli G K, Arfanis M K, *et al*., *Inorg Chem*, 56 (2017) 84.
7 Hao F, Stoumpos C C, D Cao H, Chang R P H & Kanatzidis M G, *Nat Photon*, 8 (2014) 489.
8 Amat A, Mosconi E, Ronca E, Quarti C, Umari P & Nazeeruddin M K, *et al.*, *Nano Lett*, 14 (2014) 3608.
9 Madan J, Garg S, Gupta K, Rana S, Manocha A & Pandey R, *Optik (Stuttg)*, 202 (2020) 163646.
10 Ma J, Chang J, Lin Z, Guo X, Zhou L, Liu Z, Xi H, Chen D, Zhang C & Hao Y, *J Phys Chem C*, 122 (2018) 1044.
11 Guo X, Luo G, Liu J, Liao C, Wang G & Li S, *IEEE J Photovoltaics*, 8 (2018) 1039.
12 Bala N & Mallik S K, *Indian J Pure Appl Phys*, 62 (2024) 292.
13 Amat A, Mosconi E, Ronca E, Quarti C, Umari P, Nazeeruddin M K, *et al*., *Nano Lett*, 14 (2014) 3608.
14 Guo X, Luo G, Liu J, Liao C, Wang G & Li S, *IEEE J Photovoltaics*, 8 (2018) 1039.
15 Koh T M, Krishnamoorthy T, Yantara N, Shi C, Leong W L, Boix P P, et al., *J Mater Chem*, 3 (2015) 14996.
16 Hossain M I, Alharbi F H & Tabet N, *Sol Energy*, 120 (2015) 370.
17 Haider S Z, Anwar H & Wang M, *Semicond Sci Technol*, 33 (2018) 035001.
18 Mandadapu U, Vedanayakam S V & Thyagarajan K, *Indian J Sci Technol*, 10 (2017) 1.
19 Azri F, Meftah A, Sengouga N & Meftah A, *Sol Energy*, 181 (2019) 372.
20 Kanoun A A, Kanoun M B, Merad A E & Said S G, *Sol Energy*, 182 (2019) 237.
21 Iefanova A, Adhikari N, Dubey A, Khatiwada D & Qiaoa Q, *AIP Adv*, 6 (2016) 085312.
22 Chen Y, Zhang M, Li F & Yang Z, *Coatings*, 13 (2023) 644.
23 Liu S, Biju V P, Qi Y, Chen W & Liu Z, *NPG Asia Mater*, 15(1) (2023).
24 Gheno A, Pham T T T, Bin C D, Bouclé J, Ratier B & Vedraine S, *Sol Energy Mater Sol Cells*, 161 (2017) 347.
25 Mandadapu U, Vedanayakam S V, Thyagarajan K, Reddy M R & Babu B J, *Int J Renew Energy Res*, 7 (2017) 1604.
26 Sobayel K, *et al.*, *Results Phys*, 12 (2018) 1097.
27 Owolabi J A, Onimisi M Y, Ukwenya J A, Bature A B & Ushielepan U R, *Am J Phys Appl*, 8 (2020) 8.
28 Madan J, Pandey S R & Sharma R, *Sol Energy*, 197 (2019) 212.
29 Kanoun A A, Kanoun M B, Merad A E & Goumri-Said S, *Sol Energy*, 182 (2019) 237.
30 Azri F, Meftah A, Sengouga N & Meftah A, *Sol Energy*, 181 (2019) 372.
31 Singh R, Giri A, Pal M, Thiyagarajan K, Kwak J, Lee J J, Jeong U & Cho K, *J Mater Chem A*, 7 (2019) 7151.
32 An Y, Shang A, Cao G, Wu S, Ma D & Li X, *Sol RRL*, 2 (2018) 1800126.
33 Zhang Y Y, Chen S, Xu P, Xiang H, Gong X-G, Walsh A & Wei S H, *Chin Phys Lett*, 35 (2018) 036104.
34 Meng Q, Chen Y, Xiao Y Y, Sun J, Zhang X, Han C B & Yan H, *J Mater Sci: Mater Electron*, (2020). doi: https://doi.org/10.1007/s10854-020-03029-y.
35 Wang H Y, Hao M Y, Han J, Yu M, Qin Y, Zhang P, Guo Z X, Ai X C & Zhang J P, *Chem–A Eur J*, 23 (2017) 3986.
36 Rao T P, Kumar M C S, Angayarkanni S A & Ashok M, *J Alloys Compd*, 485 (2009) 413.
37 Noman M, Shahzaib M, Jan S T, Shah S N & Khan A D, *RSC Adv*, 13 (2023) 1892.
38 Gan Y, Bi X, Liu Y, Qin B, Li Q, Jiang Q, Mo P, *Energies*, 13 (2020) 5907.
39 Jayan K D & Sebastian V, *Sol Energy*, 217 (2021) 40.
40 Wang B & Kerr L L, Nanostructured TiO2 and ZnO solar cells using CdS as sensitizer: Stability investigation. In Proceedings of the 2010 35th IEEE Photovoltaic Specialists Conference (PVSC), Honolulu, HI, USA, (2010) 001819.
41 Umar A, Tiwari P, Srivastava V, Lohia V, Dwivedi D K, Qasem H, Akbar S, Algadi H & Baskoutas S, *Micromachines*, 13 (2022) 2073.
42 Leijtens A A T, S Pathak, Teuscher J, Avolio R, Errico M, Kirkpatrik J, Ball J, Docampo P, McPherson I & Snaith H J, *Phys Chem C*, 15 (2013) 2572.
43 Zulqarnain H S, Hafeez A & Mingqing W, *Semicond Sci Technol*, 33 (2018) 035001.
44 Green M A, Emery K, Hishikawa Y, Warta W & Zou J, *Prog Photovoltaics: Res Appl*, 34 (2010) 1.